Colloid Stability and the Influence of Dissolved Gas

David R. E. Snoswell, Jinming Duan, Daniel Fornasiero, and John Ralston*

Ian Wark Research Institute, University of South Australia, Mawson Lakes, Adelaide, SA 5095 Australia

Received: July 29, 2002; In Final Form: December 10, 2002

The colloidal stability of synthetic silica spheres with clean, methylated, and dehydroxylated surfaces was studied at different concentrations of dissolved gas and KCl electrolyte at a fixed pH of 4.2. A classic stability ratio/electrolyte concentration analysis shows that hydrophobic, methylated particles undergo faster rates of aggregation with increasing concentrations of dissolved carbon dioxide. Similar data for hydrophilic particles and dehydroxylated particles show no change as a function of dissolved carbon dioxide concentration. Zeta-potential data behave similarly, showing a strong influence of dissolved gas only for methylated particles. The results are interpreted in terms of DLVO theory, with the surface-to-surface interaction dominated by the presence of very small, protruding bubbles.

Introduction

Interparticle forces in a colloidal suspension can often be described by classical DLVO theory; however, in systems where the particle surface is hydrophobic, an additional non-DLVO force is often introduced. This is an attractive force, with some studies linking its range and magnitude to the concentration of dissolved gas.[1−3] Different theories exist to explain the origin of this hydrophobic attraction, and in particular, it has been proposed that these attractive forces are due to the presence of very small bubbles on the particle surface.[4−6] The presence of small gas bubbles on hydrophobic surfaces has been demonstrated indirectly in the key early experiments of Harvey et al.[7−10] and observed on hydrophobic silica, glass, mica, and graphite surfaces using tapping-mode atomic force microscopy.[11−13] It appears that both the physical and chemical nature of the solid surface influence the hydrophobic force by promoting or suppressing the formation of very small surface bubbles.[14]

Bubble nucleation was explored in the early work of Harvey et al.[7−10] In this work, visible bubbles were shown to grow from trapped "gas pockets" on a solid surface. Harvey et al. proposed that gas nuclei form when air is trapped in surface defects during the immersion of a dry hydrophobic surface in water. Similar observations were made by Wrobel,[15] who referred to the trapped air as "submicroscopic air-bells". Indirect evidence for the presence of surface gas nuclei was provided by Wood and Sharma,[16] who demonstrated that when particles are hydrophobized in solution and not allowed to dry the range of hydrophobic attraction is greatly reduced since these "gas pockets" have no opportunity to form. Intuitively, it would seem that the amount of trapped gas on a surface should be related to the surface roughness and hydrophobicity. Indeed, a theoretical explanation by Harvey et al.[7] shows how these stable gas nuclei can form given a certain combination of advancing/receding contact angles and crevice angles. Furthermore, experimental evidence for the effect of pore size and surface hydrophobicity on bubble nucleation can be seen in the work of Ryan and Hemmingsen[17] and in the work of Lubetkin,[18] where defined pitted surfaces were investigated. The critical roles played by surface roughness and hydrophobicity in bubble nucleation are thereby demonstrated.

* Corresponding author. E-mail: john.ralston@unisa.edu.au.

Regardless of the source of these very small surface bubbles, it is evident that the reported range of hydrophobic attraction varies greatly in surface force studies, ranging from those that match DLVO theory[4,19] to studies that show long-range forces extending up to 250 nm.[20] A surface covered by very small bubbles will by nature be heterogeneous, displaying regions with different physical and chemical properties. Therefore, since only a small portion of the surfaces can interact in these experiments, a random distribution of surface bubbles may explain some of the variation observed in the measured ranges of hydrophobic attraction.

Before the advent of modern force-measurement techniques, traditional studies of aggregation rates and stability ratios allowed the indirect assessment of interparticle forces. For studies of heterogeneous surfaces, there are obvious statistical advantages in dealing with a large ensemble of particles, particularly when bulk properties such as colloid stability are to be predicted. An additional advantage of the aggregation rate approach over studies that employ fixed surfaces is the ability of the particles to rotate freely during collisions, a factor that may prove important for heterogeneous surfaces. However, despite these advantages, recent studies of this type on colloidal systems are very rare. This may be partially due to systems where classical DLVO theory fails to predict the dependence of colloid stability on electrolyte concentration accurately.[21] Recent studies have shown, however, that when the surface charge of the particles is sufficiently low classical DLVO theory adequately predicts the stability/electrolyte dependence.[22] In the case of silica, the surface charge is both low and well defined.[23]

Empirical, hydrophobic attractions are usually described using a single- or double-exponential term where one or two decay lengths are invoked.[14] Recently, a theoretical analysis by Mishchuk et al.[24] has shown that the presence of very small bubbles on the surface of a particle can lead to an attraction that appears to be similar to the action of hydrophobic forces. The origin of the effect lies in a change in the magnitude (and even the sign) of the van der Waals interactions between a particle and a macrobubble.

In this study, we investigate the effects of surface hydrophobicity and heterogeneity together with dissolved gas concentration on the stability of a colloidal particle suspension. On the

10.1021/jp021751l CCC: $25.00
Published on Web 03/11/2003

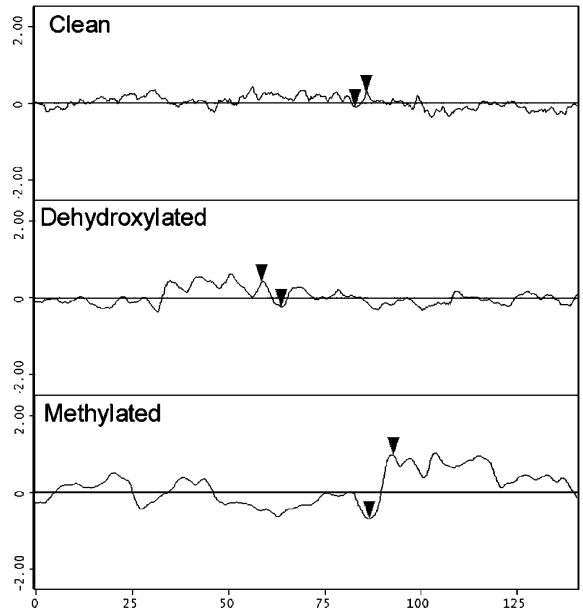

Figure 1. AFM line scans of particle surfaces. Peak-to-valley measurements for clean, dehydroxylated, and methylated particles are 0.38, 0.65, and 1.7 nm, respectively. Triangles denote the positions for the peak-to-valley measurements. All scales are given in nanometers.

basis of the premise that very small bubbles attached to particle surfaces influence hydrophobic attraction, conditions are varied to suppress or promote the formation of bubbles. The results are modeled using classical DLVO theory, introducing the influence of gas at the particle−solution interface.

Experimental Section

Materials and Reagents. High-purity (>99.9%) synthetic silica spheres were supplied by Geltech Inc. The silica spheres were cleaned in a caustic solution of KOH to remove any organic contamination,[23] followed by thorough rinsing in high-purity water. The particles had a mean diameter of 1.1 μm (standard deviation of 0.16 μm), determined by an Accusizer 770 particle-counting system. The advancing water contact angle, determined by the sessile drop technique for a similarly treated silicon wafer with a thin native oxide layer,[25] was found to be less than 5°. As further confirmation of cleanliness, a bubble cling test was performed on a submerged layer of particles in high-purity water using a video microscope.[26] No particles were found to attach to the air bubble when pressed against the layer, confirming that the particles were free from hydrophobic contaminants. The surface of these particles after cleaning was found to be very smooth, with a rms roughness of 0.16 nm as determined by atomic force microscopy (AFM) over a 100 × 100 nm area. A line scan of this surface is shown in Figure 1.

A certain quantity of these clean particles was then hydrophobized by immersion in a solution of 2% v/v trimethylchlorosilane (99+% purity) in AR-grade cyclohexane.[25] Both the particles and the silica vessels were dried in a clean oven at 110 °C prior to reaction to minimize any moisture present. After reaction, the particles were thoroughly washed in AR-grade cyclohexane to remove excess reagents and were subsequently oven dried at 110 °C. The advancing contact angle, determined by a sessile drop of water on a silicon wafer with a thin native oxide layer, treated under the same conditions, was 82°.[27] A bubble cling test showed that these particles became attached to an air bubble, confirming their hydrophobicity. The surface rms roughness, determined by AFM, was found to be 0.37 nm over a 100 × 100 nm area. A line scan of this surface is shown in Figure 1.

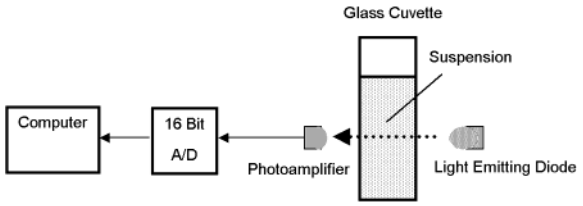

Figure 2. General arrangement of light-absorbance apparatus.

Another quantity of the cleaned particles was heated to 1050 °C for half an hour. At this temperature, substantial dehydroxylation occurs at the surface, and the surface becomes hydrophobic.[28] A silicon wafer with a thin native oxide layer was treated under the same conditions, producing a surface with an advancing water contact angle of 41°. The surface rms roughness was found to be 0.17 nm over a 100 × 100 nm area. A line scan of this surface is shown in Figure 1.

Some preliminary investigations were also performed with macrospheres, a size-exclusion chromatography packing supplied by Alltech Inc. These synthetic silica particles were porous with a nominal diameter of 7 μm and a pore size of approximately 400 nm and were chosen for their bubble nucleation potential.[17] Quantities of these particles were prepared in a fashion similar to that of the Geltech spheres. Suspensions of these particles required stirring to prevent settling.

High-purity water with a conductivity of less than 1.0×10^{-6} Ω^{-1} cm^{-1}, a pH of 5.6 ± 0.1, and a bubble residence time of less than 1 s was used throughout. Analytical-grade reagents supplied by BDH were used for the preparation of salt (KCl 99.5% purity) and acid (HCl). Food-grade carbon dioxide (99.95% purity) was passed though a suspension of precipitated silica to remove any oil or particulate contaminants prior to preparing saturated solutions. High-purity (99.997%) argon, passed through the same suspension, was also used in some preliminary experiments with macrospheres.

Equipment. To determine the rate of coagulation in the stability tests, the classical method was adopted[29,30] where the change in turbidity was measured with respect to time. A custom benchtop apparatus was fabricated specifically for this purpose. This unit used a super-high-intensity (10 000 mcd) GalnN light-emitting diode supplied by Dick Smith Electronics as the light source, with a peak wavelength of 520 nm. The amount of light transmitted through a 1-cm path length glass cuvette was then determined by the electric output of a photoamplifier (IPL 10530DAL) supplied by Integrated Photomatrix Ltd. Ambient light was excluded by a light-proof lid. During experiments, the photoamplifier voltage was recorded at 1-s intervals on a computer via a 16 bit A/D card, which resulted in a resolution of approximately 0.02 mg/dm^{-3} for the silica spheres supplied by Geltech Inc. The arrangement of this equipment is shown in Figure 2.

Throughout the experiments, a Radiometer PHM85 precision pH meter was used in conjunction with a Radiometer pHC3006-9 combined pH electrode. The meter was calibrated daily using Orion pH buffers of pH 4.00 and 7.01, which are certified as traceable to NIST standard reference material. pH readings were reproducible to within ±0.03. The probe was maintained by periodic filling with Radiometer KCl/Ag solution (part number S21M004). The temperature was maintained at 20 ± 1 °C.

A Rank Brother particle electrophoresis apparatus (Mark II) using a cylindrical cell under dark-field illumination was used

TABLE 1: Initial Intensity Gradient for the Fast Aggregation Regime and Critical Coagulation Concentrations (ccc) for Aggregation Studies of Silica Spheres at Different Dissolved Gas Concentrations[a]

condition	ccc (KCl, mM)	initial intensity gradient ± 95% confidence limits ($\times 10^{-5}$ turbidity/s)
clean, hydrophilic/normal	33	2.4 ± 0.4
clean, hydrophilic/gassed, CO_2 10^{-2} M	33	2.1 ± 0.6
dehydroxylated/normal	33	1.9 ± 0.6
dehydroxylated/gassed, CO_2 10^{-2} M	33	1.7 ± 0.4
methylated/normal	23	2.7 ± 0.8
methylated/degassed	20	2.1 ± 0.7
methylated/gassed, CO_2 10^{-2} M	20	2.3 ± 0.6

[a] Normal = under atmospheric conditions; degassed = removal of >95% of the dissolved carbon dioxide.

TABLE 2: Average Zeta Potential of Geltech Silica Spheres at pH 4.2 and a KCl Concentration of 10^{-3} M as a Function of the Dissolved Gas Concentration

particle type/conditions	average zeta potential ± 95% confidence limits (mV)
clean/degassed	−29.9 ± 1.2
clean/normal	−31.4 ± 1.0
clean/gassed, CO_2 10^{-2} M	−30.0 ± 1.3
dehydroxylated/degassed	−21.4 ± 1.1
dehydroxylated/normal	−16.7 ± 0.7
dehydroxylated/gassed, CO_2 10^{-2} M	−17.6 ± 1.6
methylated/degassed	−36.6 ± 3.6
methylated/normal	−16.4 ± 4.5
methylated/gassed, CO_2 10^{-2} M	−22.2 ± 3.7

to determine particle zeta potentials for model calculations (Figure 5). Temperature within the measurement cell was maintained at 25 °C using a thermostatically controlled water bath. Zeta potentials for relative comparison (Table 2) were obtained using a custom instrument constructed and maintained by the University of South Australia's Physics Department employing phase-analysis light scattering (PALS).[31] The temperature within this measurement cell was also maintained at 25 °C.

Atomic force microscopy (AFM) measurements of surface roughness were performed using a Nanoscope model III manufactured by Digital Instruments using tapping mode.

Methods

Particle and Solution Preparation. For each set of experiments, a concentrated stock suspension of particles was prepared in a glass cuvette with a known weight percent of particles in water. To ensure complete dispersion, the cuvette containing the suspension was immersed halfway inside a 50-W Soniclean 120T sonic bath containing approximately 200 cm^3 of water and was sonicated for 40 min. This sonication time, required to achieve optimum dispersion, was determined separately by measuring the time required to achieve a constant level of turbidity. Hydrophobic surfaces generated by methylation are known to age slowly in aqueous solutions with the advancing contact angle decreasing over time.[25,32] For this reason, hydrophobic stock suspensions were used within 5 h of preparation, within which period no time dependence was observed in the data.

Stock solutions of HCl (0.015 M), KCl (1 M) and gas-saturated water were prepared to adjust the pH, salt, and dissolved gas concentrations, respectively. In the experiments where degassed conditions were required, both the stock suspension and makeup water were placed under vacuum for a period of at least half an hour. A small Teflon stirrer placed in the evacuated solutions provided a good indication of equilibrium, nucleating no observable bubbles when the solution was sufficiently degassed. The pH of the evacuated solutions was noted to rise above 6.5 from the initial pH of 5.7. This results in a dissolved carbon dioxide concentration of less than 2% of that found under normal atmospheric conditions.[33] The stock solutions of acid and salt were not degassed since they can be concentrated by evaporation during the degassing process and generally represented less than 3 vol % of the final mixture. For each aggregation experiment, calculated portions of water, stock particle suspension, and acid and salt solutions were measured by autopipet and mixed successively. For all experiments, a constant solid concentration of 0.2 g/dm^3 was used.

A supersaturated gas solution was maintained by continuously bubbling pure carbon dioxide through water. Simultaneous measurement of pH allowed the equilibrium point to be determined and therefore the concentration of dissolved gas to be calculated.[33] Once all of the components were added to the glass cuvette, the suspension was sealed with Parafilm, hand mixed by inverting the cuvette rapidly four times, and then placed immediately in the instrument for measurement. This standard procedure was used for all experiments.

Stability Ratio. For monodispersed suspensions, Holthoff et al. have shown that if the initial particle-number concentration, wavelength, and particle size remain constant then the initial change in the light-scattering intensity at any angle is proportional to the coagulation rate constant for doublet formation.[34] Consequently, the rate of doublet formation can be expressed as eq 1.

$$k = \left(\frac{dI}{dt}\right)_{t\to 0} \frac{1}{C_f N_0 I_0} \tag{1}$$

where I is the light-scattering intensity at time t, I_0 is the initial light-scattering intensity, N_0 is the initial number concentration of particles, and C_f is a function of particle radius, incident-light wavelength, and scattering angle. The stability ratio (eq 2) is calculated by dividing the fast rate constant of aggregation, k_f, by the corresponding slow rate constant of aggregation, k_s.[37]

$$W = \frac{k_f}{k_s} \tag{2}$$

Since the parameters C_f, N_0, and I_0 remain constant in this study, the substitution of k_f and k_s by the corresponding expressions for k, given in eq 1, results in their cancellation. Therefore, the stability ratio can then be calculated by simply dividing the initial rate of change of the light-scattering intensity (or turbidity) for the fast regime by the initial rate of change of the light-scattering intensity for the slow regime as shown in eq 3.

$$W = \frac{\left(\frac{dI}{dt}\right)_{t\to 0}^{\text{fast}}}{\left(\frac{dI}{dt}\right)_{t\to 0}^{\text{slow}}} \tag{3}$$

These fast and slow rates in eq 3 are determined from the initial gradient of the turbidity−time curves.[29,30,35] Linear regression was used to obtain this gradient from the data; at least 50 data points *immediately* following cuvette insertion were used for the regression, corresponding to a time period of 50 s at the sampling rate of 1 Hz. Each regression returned R^2 values greater than 0.9. The slowest aggregation rates required up to 400 data

points to determine their gradient accurately because of an increased signal-to-noise ratio.

These rate constants were determined within the early stages of aggregation as confirmed by the calculation of the half-time of aggregation.[37] Aggregation experiments were performed with a constant initial particle concentration of 0.2 g/dm^{-3}, corresponding to an initial number concentration of 1.37×10^{14} m^{-3} as determined by Accusizer 770 measurement. This results in a half-time of approximately 1200 s at 25 °C, significantly larger than the measurement period for all experiments.

For each data set, the value of the initial intensity gradient in the fast regime was calculated as the average of at least five rates above the critical coagulation concentration (ccc). The values of this average fast rate and ccc are shown in Table 1. The values measured for the fast rates are essentially constant since any variation is within the 95% confidence limits of experimental error.

The voltage output of the photoamplifier corresponding to zero turbidity was determined by using a cuvette containing only water. Because of the fixed illumination and alignment of the instrument, the variation of this voltage was found to be negligible and was therefore taken as a constant for all experiments. Once data collection was completed, the cuvette was removed, and the solution pH was measured using a small pH probe.

Dissolved Gas Control. For all experiments, the pH was maintained at 4.2 ± 0.05. This target pH was chosen because of the formation of carbonic acid in the supersaturated carbon dioxide solutions. For 100% carbon dioxide in equilibrium with water at 1 atm of pressure, the equilibrium pH is 3.9 due to the formation of carbonic acid, corresponding to a concentration of molecular carbon dioxide (not hydrated) of 3.7×10^{-2} M.[33] When such a solution is placed under atmospheric conditions, the *effective* level of supersaturation ($([CO_2]/[CO_2]_{eq}) - 1$)) is in the order of 3200. This often leads to visible bubbles nucleating on the walls of the cuvette during measurement, which is behavior that interfered with the turbidity measurement. In addition, carbon dioxide is lost to the atmosphere under these conditions even though the exposed surface area is slight, resulting in a small pH increase during the course of the experiment.

To overcome these problems in the experiments involving elevated carbon dioxide concentrations, the initial mixture was prepared at a molecular carbon dioxide concentration of 10^{-2} M. This corresponds to a pH of approximately 4.2, an effective carbon dioxide supersaturation of 800, and an equivalent partial pressure of 0.25 at 1 atm. The target pH of 4.2 enabled a high level of supersaturation to be achieved without forming visible bubbles in the cuvette; additionally, the pH remained constant over the time period of each aggregation experiment. Because of these precautions, we are confident that accurate control of the dissolved carbon dioxide concentration was achieved. Importantly, these supersaturated solutions were also optically clear, showing no difference in turbidity from that of high-purity water. This demonstrates that dissolved gas, by itself, had no detectable effect on turbidity.

We note that it is possible to obtain an effective supersaturation level at 1 atm of 106 with argon, the next most soluble gas considered.[36] A solution saturated with argon at 1 atm can result in a dissolved gas concentration of 1.5×10^{-3} M, which is significantly lower than that achievable with carbon dioxide. The latter is therefore an "ideal gas" for achieving high levels of supersaturation at atmospheric pressure.

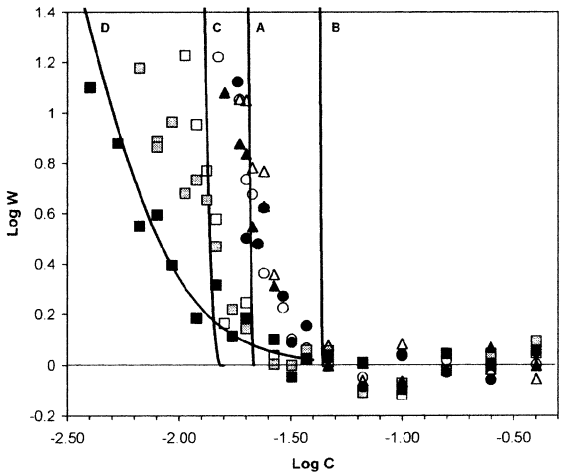

Figure 3. Stability ratio versus KCl concentration for Geltech silica spheres at pH 4.2 with a clean hydrophilic surface under normal conditions (○), a clean hydrophilic surface/dissolved CO_2 concentration of 10^{-2} M (●), methylated hydrophobic surface/normal conditions (gray squares), a methylated hydrophobic surface/dissolved CO_2 concentration of 10^{-2} M (■), methylated hydrophobic surface/degassed conditions (□), dehydroxylated surface/normal conditions (△), and a dehydroxylated surface/dissolved CO_2 concentration of 10^{-2} M (▲). Solid lines A−D indicate calculated stability curves. (Refer to Table 1 and the text for definition of "normal" and "degassed". Refer to Table 3 for the values of the parameters used in the calculation of curves A−D.)

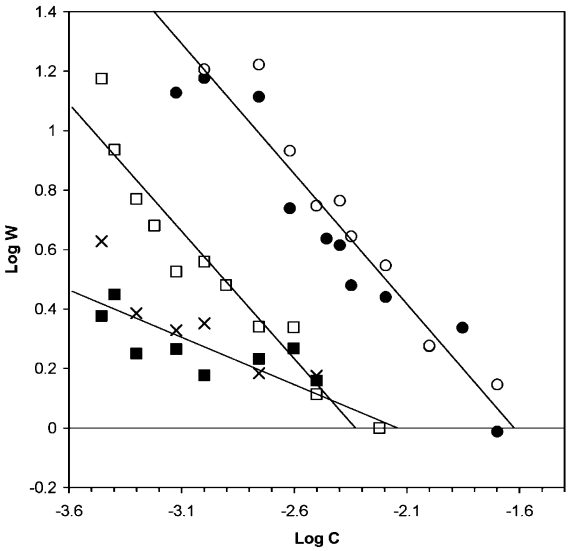

Figure 4. Stability ratio vs KCl concentration for silica macrospheres at pH 4.2 with a clean hydrophilic surface under normal conditions (○), a clean hydrophilic surface/dissolved CO_2 concentration of 10^{-2} M (●), methylated hydrophobic surface/normal conditions (□), a methylated hydrophobic surface/dissolved CO_2 concentration of 10^{-2} M (■), and a methylated hydrophobic surface/dissolved Ar concentration of 10^{-3} M (×). Straight lines denote the trends.

Results and Discussion

Stability Ratio as a Function of Dissolved Gas and Hydrophobicity. The stability ratio (W) as a function of salt concentration (C) is shown in Figures 3 and 4. The most important features of the data in Figure 3 are the variation between the curves for the particles with hydrophilic and hydrophobic surfaces and the response of these systems to increased concentrations of dissolved gas. In the case of the hydrophilic and dehydroxylated particles, it can be clearly seen that there is no detectable difference between the stability of a suspension under normal conditions compared with that of an

identical system with an increased concentration of dissolved gas. Smooth hydrophilic surfaces will wet completely on immersion in water and are not expected to nucleate very small surface bubbles under supersaturated conditions to the extent that there is any detectable impact on colloid stability. In the case of smooth dehydroxylated but hydrophobic particles where the advancing water contact angle is 41°, dissolved gas does not influence the dispersion stability. This is in accord with prior colloid probe determinations of the interaction force between dehydroxylated silica surfaces where the "jump distances" in the presence of gas-saturated (air, argon, and carbon dioxide) solutions were generally found to be less than a few nanometers.[4] Similar conclusions have been reached for smooth hydrophobic ($\theta_{ad} < 38°$) alumina surfaces.[38]

Conversely, there is a clear link between the level of dissolved gas and the stability of the suspensions where the particles have a methylated surface. First, there is a marked decrease in the gradient of the stability curve (Figure 3) as the dissolved gas concentration increases. There is an increased attraction between the particles compared with that of the clean and dehyroxylated cases. This behavior is in accord with our earlier in situ FTIR study of the aggregation behavior of smooth (a) dehydroxylated and (b) methylated 0.5-μm-diameter Geltech silica spheres at 10^{-3} M KNO_3 in the presence of carbon dioxide.[39] A second feature of note in Figure 3 is the displacement of the stability curves for the methylated silica spheres to lower critical coagulation concentration (ccc) values compared with that of the clean and dehydroxylated cases. (See also Table 1 for ccc data.) We also remark that the gradient of the log W versus log C plot for methylated particles under degassed conditions matches the gradient for the clean, hydrophilic particles.

Similar trends in the data presented in Figure 3 were also observed in a *preliminary* study of the aggregation behavior of silica macrospheres (Figure 4). The clean, hydrophilic particles show no response to the dissolved gas concentration whereas the methylated hydrophobic particles exhibit decreased stability with increasing dissolved gas concentration. Importantly, a supersaturated solution of dissolved argon also decreased the suspension stability despite the lower concentration of this gas compared with that of carbon dioxide, reflecting their different Henry constants.[36] Thus, both dissolved argon and carbon dioxide produce similar behavior. These silica macrospheres required stirring to prevent them from settling during the experiment. Because of a lack of relevant velocity and shear data as well as their porous nature, a detailed analysis of forces was not possible.

To establish whether the presence of dissolved gas influences the electrical double-layer characteristics of the particle surfaces, the zeta potential of the silica particles (clean, dehydroxylated, and methylated) was determined at pH 4.2 and 10^{-3} M KCl at various dissolved gas concentrations. The average zeta potential data, representing three separate experiments, are shown in Table 2. For the clean, hydrophilic particles, there is no influence of dissolved gas within experimental error. In the case of dehydroxylated particles, again there is no influence of dissolved gas under normal and elevated CO_2 conditions, with a slight increase only in magnitude when the system is degassed. The reason for the significant difference in zeta potential between these two silica samples lies in the dehydroxylation process. The latter removes surface charging sites, where charge can develop, as silanol groups are converted to siloxane bridges.[28,40] In the case of the methylated surfaces, there is a marked influence of dissolved gas concentration on the zeta potential when the suspensions are degassed.

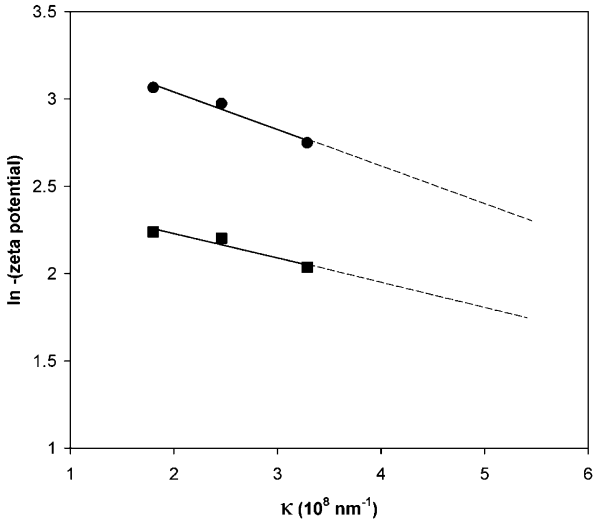

Figure 5. Zeta-potential data expressed in a plot of ln(zeta potential) vs the Debye−Huckel parameter κ at pH 4.2 using KCl electrolyte under normal conditions. (●) Clean hydrophilic particles, (■) methylated particles, and (- - -) the extrapolated region.

We have observed[41] similar behavior in our related study, where nitrogen-saturated solutions of aqueous electrolyte solution, at elevated pressures, were forced through methylated silica capillaries in streaming-potential investigations. In this study, the marked (up to 50%) change in the magnitude of the zeta potential was ascribed to the presence of very small bubbles attached to the rough (on the nanometer scale), heterogeneous (patchy) methylated silica surfaces. These bubbles could be stripped from the capillary surfaces under conditions of very high shear or prevented from forming by rendering the surface hydrophilic with a nonionic surfactant.[41]

Analysis. Classically, the forces experienced between two like particles in suspension can be described as the sum of the attractive van der Waals forces and the repulsive electrostatic forces.[42,43] In terms of interaction energies, this can be expressed as a function of H, the shortest distance between the particle surfaces.

$$V(H) = V_R(H) + V_A(H) \tag{4}$$

There are various equations describing the electrostatic repulsion as a function of distance.[42,43] The constant-charge model for identical particles shown in eq 5 was chosen since it was best able to model the experimental data. AFM colloid probe studies using similar silica spheres have also found that the constant-charge model gives the best fit to experimental data.[38,44] The approximations used for deriving eq 5 restrict its use to low surface potentials. Figure 5 demonstrates the low zeta potentials of the silica in these experiments.

$$V_R(H) = -\frac{64\pi a n k_B T}{\kappa^2}\gamma^2 \ln(1 - \exp\{-\kappa H\}) \tag{5}$$

where

$$\gamma = \tanh\frac{ze\Psi_d}{4k_B T} \tag{6}$$

In regard to eqs 5 and 6, k_B is the Boltzmann constant, T is the temperature in Kelvin, z is the valency of the ions (assuming a symmetric electrolyte), e is the electronic charge, Ψ_d is the potential at the outer Helmholtz plane, a signifies the radius of

TABLE 3: Zeta Potentials and Composite Hamaker Constants Used to Model the Stability Ratio[a]

condition	potential Ψ_d (mV)	Hamaker constant
clean hydrophilic Figure 3 curve A	$\Psi_d = -\exp[(2.15 \times 10^{-9} \times \kappa) + 3.47]$	8.4×10^{-20} J silica/vac/silica
methylated degassed Figure 3 curve B	$\Psi_d = -\exp[(2.15 \times 10^{-9} \times \kappa) + 3.47]$	particle 8.4×10^{-20} J silica/vac/silica methylation layer 0.3 nm thick 4.0×10^{-20} J layer/vac/layer
methylated degassed Figure 3 curve C	$\Psi_d = -\exp[(2.15 \times 10^{-9} \times \kappa) + 3.47]$	particle 8.4×10^{-20} J silica/vac/silica methylation layer 0.3 nm thick 4.0×10^{-20} J layer/vac/layer air layer 3 nm thick 0 J layer/vac/layer
methylated gassed CO_2 10^{-2} M Figure 3 curve D	$\Psi_d = -\exp[(1.39 \times 10^{-9} \times \kappa) + 2.51]$	particle 8.4×10^{-20} J silica/vac/silica methylation layer 0.3 nm thick 4.0×10^{-20} J layer/vac/layer composite air/water layer 3 nm thick 2.4×10^{-20} J layer/vac/layer

[a] For each calculation, the Hamaker constant for a water/vacuum/water interaction is taken to be 4.38×10^{-20} J.

the particle, n is the bulk number density of ions, and κ is the Debye−Huckel parameter with units of reciprocal length. It is generally assumed that Ψ_d and the zeta potential are similar.

When considering the attractive van der Waals forces at short distances ($H \ll a$), the interaction energy between identical particles can be adequately described by[42,43]

$$V_A = -\frac{Aa}{12H} \tag{7}$$

where A refers to the Hamaker constant for two identical particles immersed in a bathing medium.

Using these expressions, it is therefore possible to calculate the theoretical stability ratio W at any given salt concentration[42,43,45] where $s = {}^{R}/_{a}$ and R denotes the distance between the centers of the approaching spheres.

$$W = 2\int_2^\infty \exp\left\{\frac{V(s)}{k_B T}\right\} \frac{ds}{s^2} \tag{8}$$

This stability ratio was later redefined by McGown and Parfitt[46] taking into consideration the fact that the attractive van der Waals force still operates during rapid coagulation.

$$W = \frac{\int_2^\infty \exp\left\{\frac{V(s)}{k_B T}\right\} \frac{ds}{s^2}}{\int_2^\infty \exp\left\{\frac{V_A(s)}{k_B T}\right\} \frac{ds}{s^2}} \tag{9}$$

This equation can be further refined by including the factor β, proposed by Honig et al.[47] to correct for the influence of hydrodynamic interactions, which were shown to be of importance in the work of Spielman.[48]

$$W = \frac{\int_2^\infty \beta(s) \exp\left\{\frac{V(s)}{k_B T}\right\} \frac{ds}{s^2}}{\int_2^\infty \beta(s) \exp\left\{\frac{V_A(s)}{k_B T}\right\} \frac{ds}{s^2}} \tag{10}$$

where

$$\beta = \frac{6s^2 - 11s}{6s^2 - 20s + 16} \tag{11}$$

Since a theoretical plot of the stability ratio versus salt concentration can be obtained, a comparison of this theoretical plot in the slow regime below the ccc with the experimental version can be performed. By using both the Hamaker constant and surface potential as fitting parameters, the calculated stability curve can be matched to the experimental results. This has been performed recently using these equations by Puertas et al.[35] in a study of the stability of latex colloids. Although the accuracy of the Hamaker constant and surface potential obtained by this dual-parameter technique can be debated, the shape of the calculated curve does correspond very closely to the experimental curve in this particular study.[35] For the stability curves presented in the present paper, however, the particle surface potentials have been obtained from experimental results.

Using electrophoresis techniques, zeta potentials at specific salt concentrations may readily be obtained through experiments performed at KCl concentrations up to 10^{-2} M. At higher salt concentration, electrolysis becomes an issue. From a plot of ln(zeta potential) versus κ, the zeta potential near the ccc can be accessed by simple extrapolation under conditions where experimental measurements of mobility are difficult.[44] Examples of these linear extrapolations are shown in Figure 5, whereas their empirical forms are given in Table 3.

With respect to the stability curves, sensitivity analysis performed on the theoretical stability curve reveals several

important points. An increase in the Hamaker constant shifts the stability curve to lower salt concentrations but has little influence on the gradient, whereas a decrease in particle radius decreases the gradient of the curve while the ccc remains relatively constant. It is also found that any variation in the zeta potential changes both the position of the curve and, to a small degree, the gradient. This sensitivity analysis is valuable because it provides guidance in the following data interpretation.

A theoretical stability curve was determined for the clean hydrophilic particles (Figure 3, curve A). The Hamaker constant used in the calculation was adjusted to obtain the best fit with the experimental data. Values of the zeta potential and Hamaker constant that were used are given in Table 3. It is notable that the agreement between the experiment and theory for the case of hydrophilic or dehydroxylated silica is acceptable, in line with recent studies of the stability of colloidal dispersions of low surface charge.[22] The presence of *very* short range hydration forces has been detected between silica surfaces, irrespective of whether the latter are hydrophilic or dehydroxylated.[49] Under the conditions of this present study, they do not influence the essential coagulation behavior since regimes of both slow and fast aggregation are clearly evident as the salt concentration is increased.

We now address the case of methylated systems in the near-absence of dissolved gas and where gas is present. Before doing so, we remark that the evidence linking the presence of very small bubbles with surface heterogeneity (physical and/or chemical) is very strong indeed.[1,3,9,14,16,20,24] There are three reported AFM tapping-mode observations of "nanobubbles" on surfaces immersed in aqueous solutions reported to date[11−13] involving silane-treated silica or glass surfaces treated with silanes[11,13] and cleaved mica and pyrolitic graphite.[12] In only one of these studies[13] was any attempt made to quantify the surface heterogeneity through the rudimentary determination of contact angle hysteresis (substantial, at 21°, compared with that of fluoropolymer surfaces[50]). In view of the zeta-potential data in Table 2 and the observed heterogeneous nature of our methylated surfaces, the presence of very small surface bubbles would appear to influence the observed stability behavior. We have already demonstrated that various surface distributions of very small bubbles can alter the van der Waals interaction when a particle and a macrobubble interact.[24] We have no information on specific surface-bubble distributions here. We proceed, therefore, knowing that we are dealing with a statistically large number of particles and therefore use average values for methylation and gas "layer thicknesses". In the case of the methylated particles, the methylation layer thickness was taken to be 0.2 nm, representing the difference between the rms roughness data for the clean and methylated silica spheres. This value is consistent with the known chemistry of silanation processes for silica surfaces.[23,25,28]

For the case of the hydrophobic methylated particles under degassed conditions (Figure 3, curve C), it was first assumed that the observed shift in the stability curve was due to the methylation layer altering the Hamaker constant of the surface rather than to the presence of very small surface bubbles. To allow for this and any "air layer" present in later cases,[24] a more complicated model incorporating two adsorbed layers was used for the calculation of the Hamaker constant. Using the generic approach of Usui and Barouch[51] as a basis, the following equation was obtained for the case of two interacting spheres of radii a_1 and a_2 with two adsorbed layers on each particle. Figure 6 describes the nomenclature used in eqs 12−30.

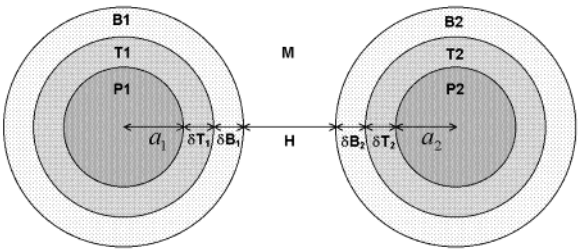

Figure 6. Arrangement of two identical spheres with a hydrophobic layer and an air layer defining the nomenclature used in eqs 12−30.

$$V_A = -\frac{1}{6}\left(\frac{a_1 a_2}{a_1 + a_2}\right)\left[\frac{A_1}{D_1} + \frac{A_2}{D_2} + \frac{A_3}{D_3} + \frac{A_4}{D_4} + \frac{A_5}{D_5} + \frac{A_6}{D_6} + \frac{A_7}{D_7} + \frac{A_8}{D_8} + \frac{A_9}{D_9}\right] \quad (12)$$

where

$$A_1 = (A_{B1}^{1/2} - A_M^{1/2})(A_{B2}^{1/2} - A_M^{1/2}) \quad (13)$$

$$D_1 = H \quad (14)$$

$$A_2 = (A_{T1}^{1/2} - A_{B1}^{1/2})(A_{B2}^{1/2} - A_M^{1/2}) \quad (15)$$

$$D_2 = H + \delta B_1 \quad (16)$$

$$A_3 = (A_{P1}^{1/2} - A_{T1}^{1/2})(A_{B2}^{1/2} - A_M^{1/2}) \quad (17)$$

$$D_3 = H + \delta T_1 + \delta B_1 \quad (18)$$

$$A_4 = (A_{B1}^{1/2} - A_M^{1/2})(A_{T2}^{1/2} - A_{B2}^{1/2}) \quad (19)$$

$$D_4 = H + \delta B_2 \quad (20)$$

$$A_5 = (A_{T1}^{1/2} - A_{B1}^{1/2})(A_{T2}^{1/2} - A_{B2}^{1/2}) \quad (21)$$

$$D_5 = H + \delta B_1 + \delta B_2 \quad (22)$$

$$A_6 = (A_{P1}^{1/2} - A_{T1}^{1/2})(A_{T2}^{1/2} - A_{B2}^{1/2}) \quad (23)$$

$$D_6 = H + \delta T_1 + \delta B_1 + \delta B_2 \quad (24)$$

$$A_7 = (A_{B1}^{1/2} - A_M^{1/2})(A_{P2}^{1/2} - A_{T2}^{1/2}) \quad (25)$$

$$D_7 = H + \delta B_2 + \delta T_2 \quad (26)$$

$$A_8 = (A_{T1}^{1/2} - A_{B1}^{1/2})(A_{P2}^{1/2} - A_{T2}^{1/2}) \quad (27)$$

$$D_8 = H + \delta B_1 + \delta B_2 + \delta T_2 \quad (28)$$

$$A_9 = (A_{P1}^{1/2} - A_{T1}^{1/2})(A_{P2}^{1/2} - A_{T2}^{1/2}) \quad (29)$$

$$D_9 = H + \delta T_1 + \delta B_1 + \delta T_2 + \delta B_2 \quad (30)$$

Using these equations, a single 0.3-nm organic layer (T1 and T2) with a Hamaker constant of 4.0×10^{-20} J (with respect to vacuum[51]) was chosen to simulate the TMCS coating since this value lies within the range reported for similar hydrocarbons.[52] The calculated stability curve for these conditions, however, does *not* explain the experimental observations; rather, the predicted displacement is to the right as a result of the lower van der Waals attraction (Figure 3, curve B).

Even under degassed conditions, some very small gas bubbles are likely to remain trapped at surface sites.[11,53] Although these sites do not constitute a uniform layer over the surface of the

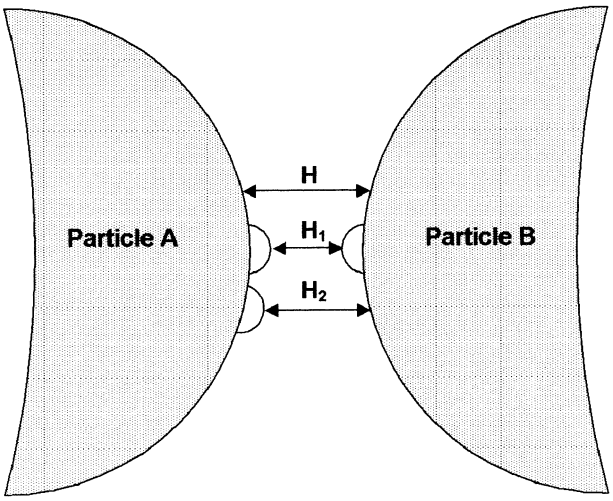

Figure 7. Scale diagram representing two 1-μm-diameter particles with 100-nm-diameter surface bubbles demonstrating the three separate interactions that can occur. In terms of the van der Waals forces, these are strongly attractive bubble−water−bubble interactions occurring over distance H_1, strongly repulsive silica−water−bubble interactions occurring over distance H_2, and attractive silica−water−silica interactions occurring over distance H.

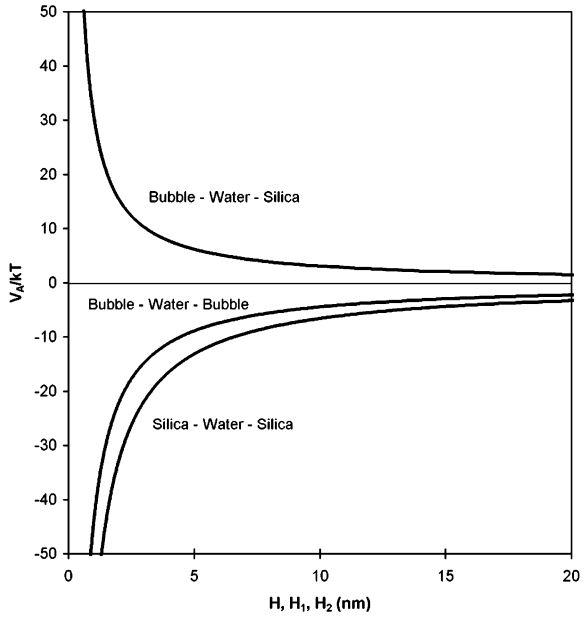

Figure 8. van der Waals energy vs distance curves for various bubble and silica interactions. For calculation purposes, the bubble size is 50 nm, the particle sizes is 500 nm, and the KCl concentration 15×10^{-3} M. Energies were calculated using eq 10 with the first- and second-layer thickness set to zero nanometers. The Hamaker constants used for the particle, water, and bubble were 8.4×10^{-20} J (silica/vac/silica), 4.38×10^{-20} J (water/vac/water), and 0 J (air/vac/air), respectively.

particle, to simplify the present calculation and allow their potential effect on the van der Waals forces to be determined, a second outer air "layer" (B1 and B2) was introduced into the calculations. If this layer is 3 nm thick, then the corresponding calculated stability curve matches the experimental curve quite closely (Figure 3, curve C).

We note that the surface potential used in our model is obtained for an ensemble of particles. The description of the surface charge distribution on a surface decorated, to some degree, with very small bubbles is not tractable at present and remains as a future problem. The recent approach of Zembala and Adamczyk[54] for particles on surfaces is very encouraging, however. The data in Table 2 and Figure 5 indicate that if the concentration of surface bubbles increases then the net effect is to decrease the magnitude of the zeta and therefore the surface potential. Although the exact potential of the gas−water interface remains elusive, studies indicate that it is likely to be rather small under the experimental conditions of this investigation.[55] The observed change in the potential of the surface covered by very small bubbles is due to the underlying solid surface being screened by these bubbles.

Given that these surface bubbles increase their coverage of the methylated surface under normal and gassed conditions, it is helpful to consider the various possible surface interactions that may occur before attempting to describe the stability curves for these remaining cases. With regard to Figure 7 , it is obvious that three distinct interactions can occur. Significantly, the bubble−water−silica van der Waals interaction is repulsive, whereas the bubble−water−bubble and silica−water−silica interactions are attractive, as shown in Figure 8. In reality, the total interaction energy between the particles will reflect a combination of these forces. The distribution of bubble coverage and diameters over the surface will further complicate any calculations. From the simplified interaction analysis, as the size and coverage of surface bubbles increase, one would expect that the bubble−water−bubble interactions would predominate. Recent AFM studies in this laboratory[53] have shown that very small bubbles on methylated silica surfaces immersed in aqueous solutions with similar electrolyte and dissolved gas levels have radii between 20 and 60 nm and a surface coverage of approximately one-half. The sizes of these bubbles are comparable to those found in another AFM study of similar surfaces.[11] As a consequence, the effective radius of interaction between the particles will be that of the protruding surface bubbles rather than that of the particles themselves (see Figure 7).

Acknowledging the problems associated with the precise determination of the Hamaker constant in this situation, we have used the following procedure to calculate curve D in Figure 3. The effective interaction radius was taken as 40 nm on the basis of extant AFM evidence.[11,53] Since the surface coverage was not known exactly, it was not possible to calculate a composite Hamaker constant with acceptable reliability by following the procedure we have used previously.[24] Hence, we have used the Hamaker constant as an effective fitting parameter while still retaining all of the other features used to calculate curve C in Figure 3. In practice, this means that the outermost layer is taken as a composite air/water region with a thickness of 3 nm. (See Table 3.) After the fitting exercise, the effective Hamaker constant for the layer B_1 (= B_2 for identical particles, Figure 6) is obtained.

Most significantly, the stability curve calculated for interacting surfaces decorated with protruding bubbles with a radius of 40 nm fits the gradient of the experimental data very closely (Figure 3, curve D). The change in the effective interaction radius caused by the protruding bubbles explains the change in the gradient of the experimental stability curves for the methylated particles as dissolved gas levels are increased (Figure 3). Furthermore, sensitivity analysis reveals that these changes in the gradient, which is the main feature of the data, cannot be explained by changes in the effective Hamaker constant because the latter does not alter the gradient.

Conclusions

The debate concerning the origin of large attractive forces, observed between hydrophobic surfaces, has continued for many

years. In our experiments, we have found that in the case of very smooth, uniform hydrophobic (dehydroxylated) and hydrophilic surfaces, classical DLVO theory can explain the interactions between these surfaces. Surface heterogeneity, both chemical and physical, and hydrophobicity promote the formation of gas bubbles. These very small surface bubbles are predicted to change both the van der Waals and electrostatic forces acting between the particles. The methylated silica particles used in this study are hydrophobic and display both chemical and physical heterogeneity. The data presented here show a clear link between the level of dissolved gas present in solution and the related colloid stability of the particles. In contrast, the colloidal stability of dehydroxylated and hydrophilic silica particles is unaffected by dissolved gas levels. The colloidal interactions have been described using an appropriate modification of DLVO theory. The analysis shows that surface-to-surface interactions between particles are dominated by the presence of very small, protruding surface bubbles.

Acknowledgment. Financial support from the Australian Research Council Special Research Centre Scheme is gratefully acknowledged. Jingwu Yang is warmly thanked for his AFM support. Fruitful discussions with Nataliya Mishchuk are warmly acknowledged.

References and Notes

(1) Considine, R. F.; Hayes, R. A.; Horn, R. G. *Langmuir* **1999**, *15*, 1657.
(2) Meagher, L.; Craig, V. S. J. *Langmuir* **1994**, *10*, 2736.
(3) Zhou, Z. A.; Zhenghe, X.; Finch, J. A. *J. Colloid Interface Sci.* **1996**, *179*, 311.
(4) Mahnke, J.; Stearnes, J.; Hayes, R. A.; Fornasiero, D.; Ralston, J. *Phys. Chem. Chem. Phys.* **1999**, *1*, 2793.
(5) Parker, J. L.; Claesson, P. M.; Attard, P. *J. Phys. Chem.* **1994**, *98*, 8468.
(6) Yakubov, G. E.; Butt, H.-J.; Vinogradova, O. I. *J. Phys. Chem. B* **2000**, *104*, 3407.
(7) Harvey, E. N.; Barnes, D. K.; McElroy, W. D.; Whiteley, A. H.; Pease, D. C.; Cooper, K. W. *J. Cell. Comp. Physiol.* **1944**, *24*, 1.
(8) Harvey, E. N.; Whiteley, A. H.; McElroy, W. D.; Pease, D. C.; Barnes, D. K. *J. Cell Comp. Physiol.* **1944**, *24*, 23.
(9) Harvey, E. N.; Cooper, K. W.; Whiteley, A. H. *J. Am. Chem. Soc.* **1946**, *68*, 2119.
(10) Harvey, E. N.; McElroy, W. D.; Whiteley, A. H. *J. Appl. Phys.* **1947**, *18*, 162.
(11) Ishida, N.; Inoue, T.; Miyahara, M.; Higashitani, K. *Langmuir* **2000**, *16*, 6377.
(12) Lou, S. T.; Ouyang, Z. Q.; Zhang, Y.; Li, X. J.; Hu, J.; Li, M. Q.; Yang, F. J. *J. Vac. Sci. Technol., B* **2000**, *18*, 2573.
(13) Tyrrell, J. W. G.; Attard, P. *Langmuir* **2002**, *16*, 6377.
(14) Ralston, J.; Fornasiero, D.; Mishchuk, N. *Colloids Surf., A* **2001**, *192*, 39.
(15) Wrobel, S. *Mine Quarry Eng.* **1952**, 313.
(16) Wood, J.; Sharma, R. *Langmuir* **1995**, *11*, 4797.
(17) Ryan, W. L.; Hemmingsen, E. A. *J. Colloid Interface Sci.* **1998**, *197*, 101.
(18) Lubetkin, S. D. *J. Appl. Electrochem.* **1989**, *19*, 668.
(19) Karaman, M. E.; Antelmi, D. A.; Pashley, R. M. *Colloids Surf., A* **2001**, *182*, 285.
(20) Christenson, H. K.; Claesson, P. M. *Adv. Colloid Interface Sci.* **2001**, *91*, 391.
(21) Hunter, R. J. *Foundations of Colloid Science*; Clarendon Press: Oxford, U.K., 1987; Chapter 7.
(22) Behrens, S. H.; Christl, D. I.; Emmerzael, R.; Schurtenberger, P.; Borkovec, M. *Langmuir* **2000**, *16*, 2566.
(23) Iler, R. K. *The Chemistry of Silica: Solubility, Polymerization, Colloid and Surface Properties, and Biochemistry*; Wiley & Sons: New York, 1979.
(24) Mishchuk, N.; Ralston, J.; Fornasiero, D. *J. Phys. Chem. A* **2002**, *106*, 689.
(25) Blake, P.; Ralston, J. *Colloids Surf.* **1985**, *16*, 41.
(26) Kitchener, J. A. *J. Soc. Cosmet. Chem. Jpn.* **1973**, *24*, 709.
(27) Crawford, R.; Koopal, L. K.; Ralston, J. *Colloids Surf.* **1987**, *27*, 57.
(28) Vansant, E. F.; Voort, P. v. d.; Vrancken, K. C. *Characterisation and Chemical Modification of the Silica Surface*; Elsevier: Amsterdam, 1995.
(29) Ottewill, R. H.; Sirs, J. A. *P. S. G. Bull.* **1957**, *10*, 262.
(30) Timasheff, S. N. *J. Colloid Interface Sci.* **1966**, *21*, 489.
(31) Thomas, J. C.; Crosby, B. J.; Keir, R. I.; Hanton, K. *Langmuir* **2001**, *18*, 4243.
(32) Laskowski, J.; Kitchener, J. A. *J. Colloid Interface Sci.* **1969**, *29*, 670.
(33) Butler, J. N. *Carbon Dioxide Equilibria and Their Applications*; Addison-Wesley: Reading, MA, 1982; Chapter 2.
(34) Holthoff, H.; Egelhaaf, S. U.; Borkovec, M.; Schurtenberger, P.; Sticher, H. *Langmuir* **1996**, *12*, 5541.
(35) Puertas, A. M.; Nieves, F. J. *J. Colloid Interface Sci.* **1999**, *216*, 221.
(36) *CRC Handbook of Chemistry and Physics*, 83rd ed.; Lide, D. R., Ed.; CRC Press: Boca Raton, FL, 2002.
(37) Gregory, J. *Crit. Rev. Environ. Control* **1989**, *19*, 185.
(38) Larson, I.; Drummond, C. J.; Chan, D. Y.; Grieser, F. *J. Phys. Chem.* **1985**, *16*, 41.
(39) Gong, W.; Stearnes, J.; Fornasiero, D.; Hayes, R. A. *Phys. Chem. Chem. Phys.* **1999**, *1*, 2799.
(40) Grieser, F.; Lamb, R. N.; Wiese, G. R.; Yates, D. E.; Cooper, R.; Healy, T. W. *Radiat. Phys. Chem.* **1984**, *23*, 43.
(41) Churaev, N. V.; Ralston, J.; Sergeeva, I. P.; Sobolev, V. D. *Adv. Colloid Interface Sci.* **2002**, *96*, 265.
(42) Derjaguin, B. V.; Churaev, N. V.; Muller, V. M. In *Surface Forces*; Kitchener, J. A., Ed.; Plenum Publishing: New York, 1987.
(43) Elimelech, M.; Gregory, J.; Jia, X.; Williams, R. *Particle Deposition and Aggregation*; Butterworth-Heinemann: Oxford, U.K., 1995.
(44) Toikka, G.; Hayes, R. A. *J. Colloid Interface Sci.* **1997**, *191*, 102.
(45) Ortega-Vinuesa, J. L.; Martin-Rodriguez, A.; Hidalgo-Alvarez, R. *J. Colloid Interface Sci.* **1996**, *184*, 259.
(46) McGown, D. N. L.; Parfitt, G. D. *J. Phys. Chem.* **1967**, *71*, 449.
(47) Honig, E. P.; Roebersen, G. J.; Wiersema, P. H. *J. Colloid Interface Sci.* **1971**, *36*, 97.
(48) Spielman, L. A. *J. Colloid Interface Sci.* **1970**, *33*, 562.
(49) Grabbe, A.; Horn, R. G. *J. Colloid Interface Sci.* **1992**, *157*, 375.
(50) Schneemilch, M.; Welters, W. J. J.; Hayes, R. A.; Ralston, J. *Langmuir* **2000**, *16*, 2924.
(51) Usui, S.; Barouch, E. *J. Colloid Interface Sci.* **1989**, *137*, 281.
(52) Hough, D. B.; White, L. R. *Adv. Colloid Interface Sci.* **1980**, *14*, 3.
(53) Yang, J.; Duan, J.; Fornasiero, D.; Ralston, J. *J. Phys. Chem. B*, accepted for publication, 2003.
(54) Zembala, M.; Adamczyk, Z. *Langmuir* **2000**, *16*, 1593.
(55) Hewitt, D.; Fornasiero, D.; Ralston, J.; Fisher, L. R. *J. Chem. Soc., Faraday Trans. 1* **1993**, *89*, 817.